33rd Annual International Conference of the IEEE EMBS
Boston, Massachusetts USA, August 30 - September 3, 2011

Chronic behavior evaluation of a micro-machined neural implant with optimized design based on an experimentally derived model

Alexandru Andrei, Marleen Welkenhuysen, Lieveke Ameye, Bart Nuttin and Wolfgang Eberle

Abstract— **Understanding the mechanical interactions between implants and the surrounding tissue is known to have an important role for improving the bio-compatibility of such devices. Using a recently developed model, a particular micro-machined neural implant design aiming the reduction of insertion forces dependence on the insertion speed was optimized. Implantations with 10 and $100\,\mu m/s$ insertion speeds showed excellent agreement with the predicted behavior. Lesion size, gliosis (GFAP), inflammation (ED1) and neuronal cells density (NeuN) was evaluated after 6 week of chronic implantation showing no insertion speed dependence.**

I. INTRODUCTION

Implantable neural micro-systems based on silicon technology provide an interface to the nervous system with cellular resolution to physiological processes unattainable today using classical microwires or non-invasive methods. However, even if significant advances had been made towards impressive recording functionality with active circuit integration [1], ultimately most devices lose their functionality within months or even weeks after implantation due to tissue reactive response that leads to cellular sheath encapsulation. Tissue response to foreign implanted bodies evolves from an acute response triggered by the initial tissue damage that causes astrogliosis spreading few hundred of micrometers towards a more compact sheath around the implant extending few tens of micrometers [2] that blocks neurite growth and axonal regeneration [3]. Moreover, the persistently activated microglia around the implant were assumed to be a source of neurotoxicity, the resulting neuronal death and degeneration taking place along additional tens of micrometers beyond the sheath [4], [5]. Significant tissue deformation and blood vessel damage occurs during the implantation procedure itself [6]. The implant geometry and insertion speed have been shown to be closely related to this deformation [6], the insertion forces [7], [8], [9], [10] as well as to the acute and chronic tissue response [5], [2], [11]. However, most of these studies evaluated the contributions of only one or two parameters at a time, while fixing the rest. A quantitative comparison proved to be difficult especially since one-at-a-time factor values sweep methods having little chance to detect interactions between factors, making the extrapolation of the results to different geometries that have not been tested before hazardous. In this context, a recently developed experimental response surface model pointed out the presence of important interaction effects between the implant's chisel shape tip angle, shaft width, thickness and insertion speed when it comes to their impact on the insertion forces and tissue dimpling [12]. These interactions showed that for particular configurations, one can safely increase certain factors without causing unwanted significant force or tissue dimpling increase. In the present study, the abovementioned model has been used for a micromachined implant geometry optimization aiming the reduction of the insertion forces and tissue dimpling while increasing the insertion speed from $10\mu m/s$ to $100\mu m/s$. Faster insertion speeds are suitable for screening of a large number of animals and chronic experiments, where generally the reduction of the overall surgery time is desired. The tissue response was evaluated after 6 weeks of implantation by estimating the amount of gliosis, inflammation, and neuronal cell loss with immunohistochemistry.

A. Andrei is with the Bioelectronic Systems Group, Imec, 3001 Heverlee, Belgium andreial@imec.be

M. Welkenhuysen is with the Laboratory of Experimental Functional Neurosurgery, Department of Neurosciences, K. U. Leuven, 3000 Leuven, Belgium welkenh@imec.be

L. Ameye is with the Department of Electrical Engineering, K. U. Leuven, 3001 Heverlee, Belgium lieveke.ameye@hotmal.com

B. Nuttin is with the Laboratory of Experimental Functional Neurosurgery, Department of Neurosciences, K. U. Leuven, 3000 Leuven, Belgium bart.nuttin@uzleuven.be

W. Eberle is with the Bioelectronic Systems Group, Imec, 3001 Heverlee, Belgium eberle@imec.be

II. MATERIALS AND METHODS

A. Micromachined neural implant manufacture

The neural implants manufacture started with the reactive ion etching of a 1 cm long, $200\,\mu m$ wide rectangular pattern onto the front side of a thermally oxidized silicon wafer. This defined the overall shape of the neural implant and had on one end a triangular sharp tip with a 20° opening angle. The silicon oxide etch was followed by a Bosch type deep silicon etch process to a final depth of $170\,\mu m$. The resulting chisel point tip shape displayed perfectly straight side-wall profiles. After the wafers have been flipped upside down and bonded on dedicated carrier wafers, a wafer thinning process has been applied on their backside until their overall thickness was reduced to $100\,\mu m$. Given the fact that the final wafer thickness was lower that the front side deep silicon etch depth, the thinning process defined in the same time the final $100\,\mu m$ thickness of the neural implants and separated them from the rest of the wafer by opening the front side etch grooves. After the devices were released from the carrier, they were coated with a $1\,\mu m$ thick parylene C layer that provided excellent conformity and helped reducing the typical sub-micron Bosch type process side-wall roughness. Fig.1 shows the final neural implant device, connected to a dedicated package and ready for implantation.

978-1-4244-4122-8/11/$26.00 ©2011 IEEE

B. Implantation and force measurements

The 12 young male Wistar rats (+/- 250 g) used in this experiment were placed under general anesthesia by chloral hydrate (0.5 g/kg rat s.c.) in a stereotaxic frame so that bregma and lambda were in the same horizontal plane, and a heating blanket preventing hypothermia during the surgery. Local anesthesia was used before scalp incision after shaving and disinfecting with isopropyl alcohol. A 3 mm diameter craniotomy of was performed after visualization of bregma. Possible bone chips were washed away with steril saline until the dura surface was clean. The dura was carefully cut and retracted in such a way that the center of the exposed pia surface remained clean and undamaged. The packaged neural implant was fixed on a holder making sure that its shaft was vertical and was lowered into the tissue at constant speed using a hydraulic micro-drive. An equal number of 6 implantations were performed for the slowest $10\,\mu m/s$ and the fastest $100\,\mu m/s$ insertion speeds with randomized implantation order and the surgeon blinded for the experimental parameters. Axial forces were recorded by a miniature load cell mounted vertically between the micro-drive rod and the neural implant holder. The set-up showned in Fig. 1 was placed on an anti-vibration table inside a grounded Faraday cage. After contacting the tissue surface, the force increased until it reached a maximum value corresponding to the penetration of the pia mater. After the abrupt force value decrease that followed corresponding to a tissue spring back and partial strain relaxation, the force values continued to increase until the target 9 mm subdural depth was reached. The stop of the implant movement led to tissue relaxation and recorded force values decrease and stabilization. Fig. 1 shows an example of such an insertion force measurement. As for similar literature studies [7], [8], four experimental outcome values were defined for each insertion experiment: the penetration force (F_{in}), its corresponding depth indicating the amount of dimpling (D_{in}), the end of the insertion force (F_{end}) and the sustained force value after 3 minutes tissue relaxation (F_{rest}). Only one probe was used for each rat, all implantations being performed in the ventromedial nucleus of the hypothalamus (VMH, coordinates: 3 mm posterior of bregma, 1 mm left to the mid-line and 9 mm ventral of the dura mater [13]). These coordinates were chosen as the implant site, based on the absence of ventricles in the implantation track and the sufficient subdural depth to accommodate the 10 mm long probes. Implants were fixed to the skull with dental cement and the wound was sutured. All experiments were carried out in accordance with the protocols approved by the ethical committee of the KULeuven, Belgium and with the legal requirements of our national authority.

C. Histology and image analysis

After 6 weeks, the animals were euthanized with an overdose Nembutal and were perfused intracardially with 10% sucrose and 4% formaldehyde in distilled water followed by the resection of the brain. Brains were kept in 4% formaldehyde in distilled water overnight, transferred

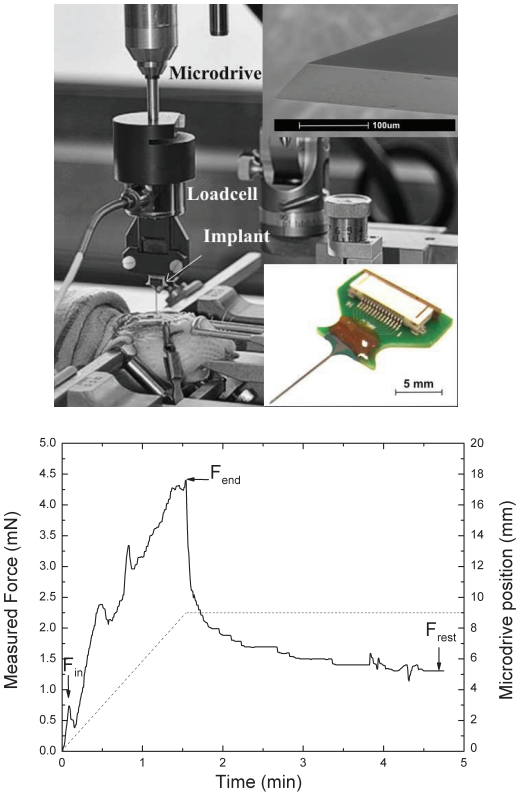

Fig. 1. Pictures of a packaged neural implant and experimental stereotaxic insertion set-up (top). An example of the insertion force measured as a function of time for a $100\mu m/s$ insertion speed (bottom).

to phosphate buffered saline (PBS) with 20% sucrose, and preserved at $4°C$. The frozen brains were cut in $20\,\mu m$ thick transversal slices with a cryostat. Three slices from similar depths ($1000\,\mu m$ in the cortex, $5800\,\mu m$ in the middle, i.e. the thalamus, and $8500\,\mu m$ near the tip) per rat were collected and stained with Nissl stain (Cresylviolet, to verify subdural depth) or prepared for immunohistochemistry. The slices were incubated with primary antibodies rabbit GFAP to assess activated astrocytes and gliosis (Dako), mouse ED1 for activated microglia/macrophages and inflammation evaluation (Abcam) and mouse NeuN for neuronal density (Millipore). Alexa-444 and Alexa-568 fluorescently labeled secondary antibodies (Molecular Probes) were diluted in blocking solution in PBS and incubated for 4 hours at room temperature. Sections were mounted with Vectashield and sealed. Fluorescent images were collected using an Axiocam HSc camera attached to a LSM5 Pascal microscope with a Plan-Apochromat $5 \times /0.16$ lens. An 8 bit grayscale image was captured for each specimen, the implant site being centered in the camera field and oriented identically for all specimens. Using the same exposure time, an image corresponding to the same coordinates was captured from the contralateral hemisphere for each sample. To quantify the extent of the reactivity, the average fluorescence intensity was determined with ImageJ from three areas corresponding to $100\,\mu m$ wide areas starting from the probe-tissue interface up to a distance of $500\,\mu m$. The values were adjusted to

the background fluorescence intensity of the control image obtained from the same area of the undamaged contralateral hemisphere. The obtained data was analyzed using non-parametric statistical tests. Special care was taken in order to correct for the dependency between multiple observations per rat by using a generalized estimating equations modeling method instead of the commonly used ANOVA.

D. Implant geometry optimization

Chisel point type micromachined neural implants geometry can be defined by three parameters: the tip angle (A) along with the shaft width (W) and thickness (T). A recently developed experimental model [12] showed that the insertion forces F_{in}, F_{end}, F_{rest} and tissue dimpling D_{in} could be related to A, W, T and the insertion speed S by the means of a polynomial model that includes linear relations, first order factor integrations (any multiplication between two factors) and second order curvature terms. A and S were found to be the main factors influencing F_{in} and D_{in}. Minimizing either of these two factors opened the opportunity of safely increasing the other. However, A no longer played a significant role for F_{end} and F_{rest}. These force values were mainly depended of W and S, factors expressing the friction forces between the implant side-walls and the brain tissue. An increase of W would increase the tissue compression and therefore an increase of the forces normal to the lateral surface of the probe, leading ultimately to higher friction forces. Reducing the insertion speed proved to be the most efficient way of reducing F_{end}, while F_{rest} could be reasonable reduced by either decreasing S or W. In the light of these results, the least insertion speed sensitive neural implant design would be one that minimizes the tip angle and shaft width. 20° was found to be a good compromise for A, between a reduced F_{in} and D_{in} speed dependence and the possibility to accommodate recording electrodes close enough to the tip. Furthermore, it was shown in literature that 5° tip angles had higher chances of causing blood vessel severing and rupture [6]. $200\mu m$ was the minimal width necessary for the placement and routing of $50\,\mu m$ diameter electrodes in tetrode configuration.

III. RESULTS AND DISCUSSION

Fig. 2 shows excellent agreement between the behavior predicted by the model used for the implant geometry optimization and the two groups of measurements performed in the current study. As expected, the 20° tip angle reduced the impact that the insertion speed increase from $10\,\mu m/s$ to $100\,\mu m/s$ would have had on F_{in} and D_{in} to the point that no statistically significant difference could be observed between the two groups. This was not the case for F_{end}, where the predicted $3\times$ increase occurred and led to a statistically significant higher force values for the fast insertions. The tissue compressive reaction force after the 3 minutes of relaxation (F_{rest}) was not significantly higher for the $100\,\mu m/s$ group, the significant values spread being higher than the expected F_{rest} change. The dashed lines in Fig. 2 show what the predicted F_{end} and F_{rest} values were for a $400\,\mu m$ wide implant: about two times higher regardless of the insertion speed. The tissue lesion observed during histology usually had the square shape of the shaft cross implant cross section as shown in Fig. 3. Its size was not affected by the insertion speed. The extent of gliosis (GFAP) was almost 30% higher near the implant ($0-100\,\mu m$ area), significant differences when compared with the control image being detected as far as $500\,\mu m$ (3% increase for the $400-500\,\mu m$ area). The presence of activated macrophages (ED1) was significatlly higher (11% increase for the $0-100\,\mu m$ area) than the control image up to $200\,\mu m$ from the probe-tissue interface. The distance to the implant was found to have no significant influence on the NeuN reactivity, the neuronal cells density in the vicinity of the probe being comparable to undamaged tissue. However, certain regions in the cortex displayed sometimes very low neuronal density, real "kill zones" that were not observed deeper along the shaft or near the tip of the implants. This depth dependent behavior was not observed for either GFAP or ED1. No significant differences between the fast and slow insertion groups were observed for any of the three stainings. Furthermore, the histological results had no significant correlation with the insertion forces and tissue dimpling values. Reduced GFAP reactivity has been reported in literature for an experiment where the insertion speed of a rather blunt implant $(A = 50^\circ)$ was decreased from $820\,\mu m/s$ down to $0.42\,\mu m/s$ [11]. The two possible explanations for the lack of insertion speed influence on the chronic tissue response observed in our study could be either the more limited insertion speed range $(10-100\,\mu m/s)$ and/or our sharper tip design. The latter assumption could be supported by the lack of significant increase of tissue dimpling with the insertion speed, a behavior that we demonstrated to be a direct consequence of the 20° tip angle. Reducing the insertion speed influence on the insertion forces and tissue dimpling was the objective of our study. However, this might also be the very reason of the lack of correlation between the insertion behavior and the histological results, a question that will be answered in future studies.

IV. CONCLUSION

A recently developed experimental model capable of predicting micromachined neural implants insertion behavior has been used for choosing the implant geometry less sensitive to insertion speed by reducing the tip angle and shaft width. The insertion experiments showed excellent agreement with the predicted behavior. Increasing the insertion speed from 10 to $100\,\mu m/s$ led to a significant increase only for the 9 mm deep end of insertion force. However, this increase proved to have no influence on the chronic tissue reaction, the lesion size, gliosis (GFAP), inflammation (ED1) and neuronal cells density (NeuN) being uncorrelated to the insertion speed and measured forces. The rapid decrease of inflammation from the implant-tissue interface as well as the uniform neuronal cells presence in the close vicinity of the probe demonstrated the good chronic bio-compatibility of the neural implant.

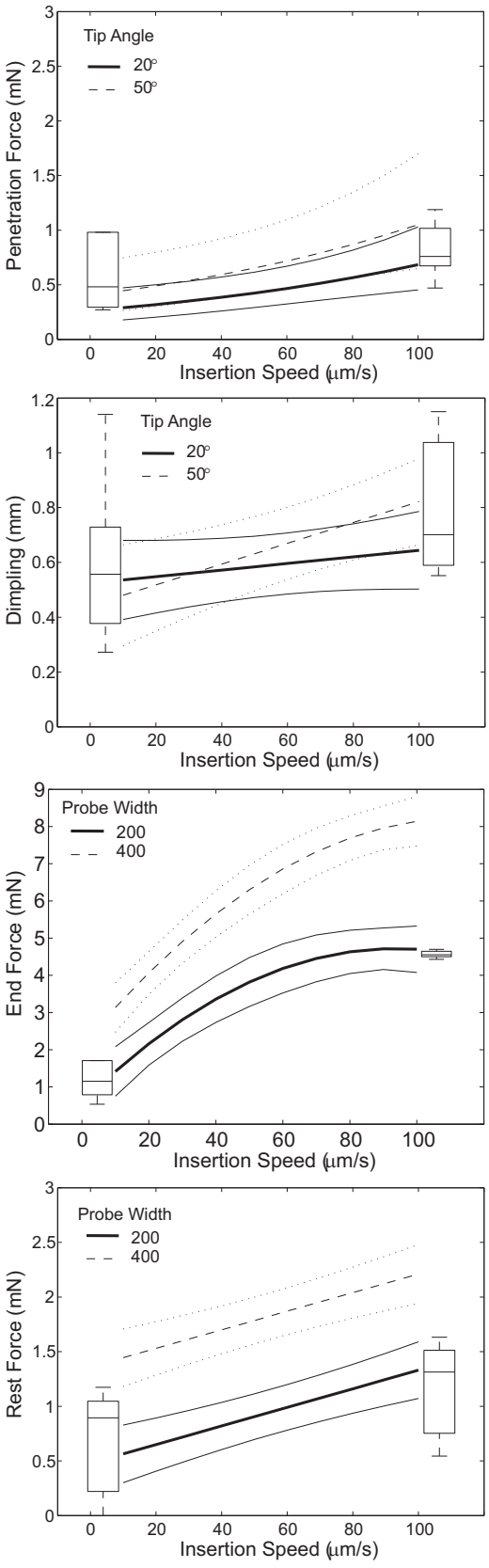

Fig. 2. Comparison between the predicted insertion behavior (full thick lines - with 95% confidence interval boundaries in thin lines) according to [12] and the current study results for the $10\,\mu m/s$ and $100\,\mu m/s$ insertion speeds (box plots) and $A = 20°$, $W = 200\,\mu m$ and $T = 100\,\mu m$ geometry. Other unfavorable implant geometries ($A = 50°$ or $W = 400\,\mu m$) model predictions are shown in dashed lines.

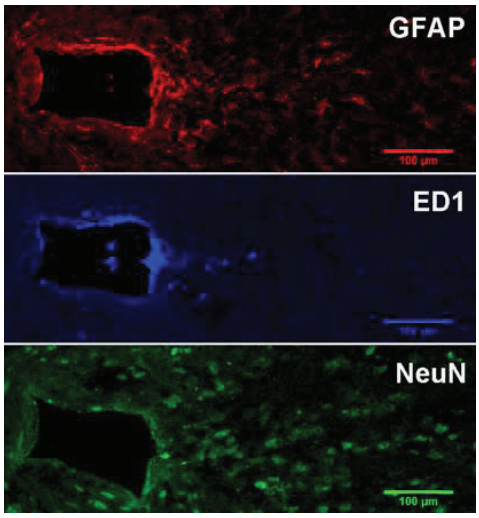

Fig. 3. Representative immunoreactivity images of the tissue chronic implantation lesion around the tip of the neural probe. Brightness and contrast have been enhanced for visualization purposes.

REFERENCES

[1] K. D. Wise, A. M. Sodagar, Y. Yao, M. N. Gulari, G. E. Perlin, and K. Najafi, "Microelectrodes, microelectronics, and implantable neural microsystems," *Proceedings of the IEEE*, vol. 96, no. 7, pp. 1184–1202, 2008.

[2] D. Szarowski, M. D. Andersen, S. Retterer, A. Spence, M. Isaacsonc, H. Craighead, J. Turner, and W. Shain, "Brain responses to micro-machined silicon devices," *Brain Research*, vol. 983, pp. 23–35, 2003.

[3] J. Silver and J. H. Miller, "Regeneration beyond the glial scar," *Nature Reviews Neuroscience*, vol. 5, pp. 146–56, 2004.

[4] R. Biran, D. C. Martin, and P. A. Tresco, "Neuronal cell loss accompanies the brain tissue response to chronically implanted silicon microelectrode arrays," *Experimental Neurology*, vol. 195, pp. 115–26, 2005.

[5] D. J. Edell, V. V. Toi, V. M. McNeil, and L. D. Clark, "Factors influencing the biocompatibility of insertable silicon microshafts in cerebral cortex," *IEEE Transactions on Biomedical Engineering*, vol. 39, pp. 635–643, 1992.

[6] C. S. Bjornsson, S. J. Oh, Y. A. Al-Kofahi, Y. J. Lim, K. L. Smith, J. N. Turner, S. De, B. Roysam, W. Shain, and S. J. Kim, "Effects of insertion conditions on tissue strain and vascular damage during neuroprosthetic device insertion," *Journal of Neural Engineering*, vol. 3, pp. 196–207, 2006.

[7] W. Jensen, K. Yoshida, and U. G. Hofmann, "In-vivo implant mechanics of flexible, silicon-based acreo microelectrode arrays in rat cerebral cortex," *IEEE Transactions on Biomedical Engineering*, vol. 53, pp. 934–940, 2006.

[8] N. H. Hosseini, R. Hoffmann, S. Kisban, T. Stieglitz, O. Paul, and P. Ruther, "Comparative study on the insertion behavior of cerebral microprobes," in *IEEE EMBS*, IEEE, Ed., vol. 29, 2007, pp. 4711–4714.

[9] A. A. Sharp, A. M. Ortega, D. Restrepo, D. Curran-Everett, and K. Gall, "In vivo penetration mechanics and mechanical properties of mouse brain tissue at micrometer scales," *IEEE Transactions on Biomedical Engineering*, vol. 56, pp. 45–53, 2009.

[10] A. Andrei, M. Welkenhuysen, M. Gonzalez, and W. Eberle, "Insertion mechanics of silicon-based neural implants for rodents," in *ESB*, vol. 17, 2010.

[11] A. A. Sharp, H. V. Panchawagh, A. Ortega, R. Artale, S. Richardson-Burns, D. S. Finch, K. Gall, R. L. Mahajan, and D. Restrepo, "Toward a self-deploying shape memory polymer neuronal electrode," *Journal of Neural Engineering*, vol. 3, pp. L23–L30, 2006.

[12] A. Andrei, M. Welkenhuysen, B. Nuttin, and Wolfga, "A model predicting the in-vivo insertion behavior of micromachined neural implants," *Journal of Neural Engineering*, p. submitted paper, 2011.

[13] G. Paxinos and C. Watson, *The Rat Brain in stereotaxic coordinates*, 6th ed., A. Press, Ed. Elsevier, 2007.